COMMUNICATION

Check for updates

Transport of partially active polymers in chemical gradients†

Shashank Ravichandir, [ID] [ab] Bhavesh Valecha, [ID] [c] Pietro Luigi Muzzeddu, [ID] [d] Jens-Uwe Sommer [ID] *[ab] and Abhinav Sharma [ID] *[ac]

The transport of molecules for chemical reactions is critically important in various cellular biological processes. Despite thermal diffusion being prevalent in many biochemical processes, it is unreliable for any sort of directed transport or preferential accumulation of molecules. In this paper, we propose a strategy for directed motion in which the molecules are transported by partially active polymeric structures. These polymers are assumed to be Rouse chains, in which the monomers are connected *via* harmonic springs and these chains are studied in environments that have activity varying spatially. The transport of such polymers is facilitated by these chemical/activity gradients which generate an effective drift. By marginalizing out the active degrees of freedom of the system, we obtain an effective Fokker–Planck equation for the Rouse modes of the polymer. In particular, we solve for the steady state distribution of the center of mass and its mean first passage time to reach an intended destination. We focus on how the arrangement of active units within the polymer affects its steady-state and dynamic behavior and how they can be optimized to achieve high accumulation or rapid motility.

Chemical gradients are ubiquitous in biological systems across length scales. These gradients help in carrying out chemical reactions, mechanical work, and biological interactions,[1] which include growth and migration of cells, healing of wounds, cancer metastasis,[2] and in the positioning of nuclei within cells.[3] Polymers also play a prominent role in microbiological processes. These include DNA transcription and replication where DNA/RNA polymerases move along the DNA,[4,5] the dynamics of chromosomal loci[6,7] and chromatin,[8] arrangement

a Institut Theory der Polymere, Leibniz-Institut für Polymerforschung, 01069 Dresden, Germany
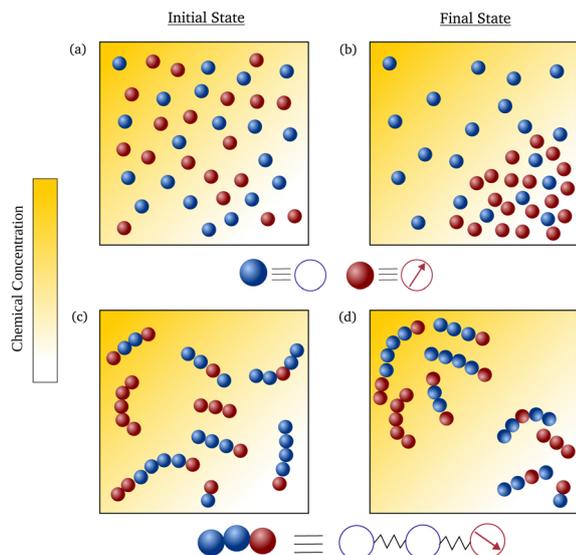
b Institut für Theoretische Physik, Technische Universität Dresden, 01069 Dresden, Germany. E-mail: jens-uwe.sommer@tu-dresden.de

c Institut für Physik, Universität Augsburg, 86159 Agusburg, Germany. E-mail: abhinav.sharma@uni-a.de

d Department of Biochemistry, University of Geneva, 1211 Geneva, Switzerland

† Electronic supplementary information (ESI) available. See DOI: https://doi.org/10.1039/d4sm01357c

of eukaryotic genome,[9] formation of cell organelles *via* phase separation,[10,11] among many others.

In biology, biopolymers often function in active[12–18] environments. For example, myosin motors actively stress the actin network in the cytoskeleton,[19] while kinesin motors transport cargo along microtubules.[20–22] Rather than being uniformly active, these polymers are active at specific locations. Inspired by such systems, this work explores a potential structure–function relationship in active–passive hybrid polymers, specifically, how such partially active polymers can facilitate the targeted transport of molecules. It is important to recognize that the term active polymers is also used for polymers in non-equilibrium surroundings like bacterial baths and there have been various studies that look into the structural and dynamical properties of both interpretations of active polymers.[23–39] However, it is only recently that self-localization of these polymers in response to chemical gradients has received some attention.[40,41] In this work we consider polymer molecules that are inherently active and self-propelled due to a fuel/activity field.

Consider an environment, in which there are gradients in the fuel concentration, leading to space-dependent activity,[42,43] filled with a mixture of active (the carriers) and passive (the molecules to be delivered to their intended destinations) monomers. We consider a scenario where monomers can link together to form composite polymers that are modeled as Rouse chains consisting of both active and passive units as shown in Fig. 1. The passive and active monomeric units are modeled as simple Brownian particles and active Brownian particles (ABPs), respectively. We do not assume a specific mechanism of activity but consider a scenario where a particle's activity is proportional to the local concentration.[44] We assume gradients are small, and therefore activity remains effectively constant on the particle's length scale, and no directional cue is present. The choice of ABPs is motivated by the fact that it is a simple model that is also used to describe self-propelled colloidal molecules[45–47] that can be synthesized in labs.[44,48–52] It has been analytically demonstrated that individual ABPs, in

Fig. 1 (a) A mixture of active (red spheres) and passive (blue spheres) particles in an inhomogeneous environment. These spheres can either be representative of colloidal particles or coarse-grained molecules. (b) In absence of interparticle interactions, the passive particles will remain homogeneously distributed, wheras the active particles will accumulate in low activity regions. (c) The active and passive particles can connect to each other to form polymeric structures, which are modeled as Rouse chains. (d) These partially active polymers preferentially accumulate in low or high activity regions based on their structures. Note: these are schematic snapshots that do not give any information on the degree of self-localization.

the presence of gradients, accumulate in regions of low fuel concentration or activity.[53,54] This is in contrast to some living systems, *e.g.* the bacterium *E. coli* which moves up the activity gradient by altering its tumble rate,[55] thus leading to chemotaxis.[56,57] Though there have been some studies on the transient behavior of ABPs leading to the phenomenon of "pseudochemotaxis",[58–62] this did not lead to any sort of preferential accumulation in regions of high activity. However, recent works[40,63–66] have shown that connected structures with single or multiple ABPs can show chemotactic behaviour, the principles of which we'll be building upon.

In the present work, we address the following questions: (i) does the number and location of active monomers in a polymer affect its preferential accumulation? (ii) Are the polymer chains that localize most effectively also the fastest in getting to the target region? Investigating these will help us understand the static and dynamic accumulative behavior of active–passive hybrid polymers. We also show that the results of this work are unaffected by the model of activity of the particles, and hence, could give insights into the transport of molecules for various bio-chemical processes.

We model the active–passive hybrid polymers as Rouse chains, in which the interacting monomers are connected to each other *via* harmonic springs of stiffness ζ. For a polymer of chain length N, the activities are assigned by the binary variables $\{\alpha_i\}$, with $i = \{0, 1\cdots N-1\}$. Specifically, $\alpha_i = 1$ if the i-th monomer is active and $\alpha_i = 0$ otherwise. The overdamped

Langevin equations describing the stochastic dynamics of the positions $\{X_i(t)\}$ and orientation unit vectors $\{p_i(t)\}$ of individual monomers are:

$$\dot{X}_i(t) = -\mu\nabla_{X_i}\mathscr{H} + \mu\alpha_i f_s(X_i)p_i + \xi_i(t),$$

$$\dot{p}_i(t) = p_i \times \eta_i(t), \tag{1}$$

where μ is the mobility of the particle, f_s is the swim force due to the spatially varying fuel concentration or activity field, $\{\xi_i(t)\}$ and $\{\eta_i(t)\}$ are zero-mean white Gaussian noises with correlations $\langle\xi_i(t) \otimes \xi_j(s)\rangle = 2DI\delta_{ij}\delta(t-s)$ and $\langle\eta_i(t) \otimes \eta_j(s)\rangle = 2D_r I\delta_{ij}\delta(t-s)$. Here $\otimes$ represents the outer product, D and D_r are the translational and rotational diffusive coefficients, respectively, and I is the $d \times d$ identity matrix, d being the number of dimensions. The Hamiltonian $\mathscr{H}$ modeling the spring interactions between particles is

$$\mathscr{H} = \frac{\zeta}{2}\sum_{ij} M_{ij}X_i \cdot X_j, \tag{2}$$

where M_{ij} is the connectivity matrix[67] for the polymer chain. Even though the relations we derive are applicable for a general connectivity matrix, we will be restricting our study to linear polymer chains, *i.e.*, M_{ij} is a tridiagonal matrix. We write down the Fokker–Planck equation[68,69] in terms of the Rouse modes $\{\chi_i\}$[70] obtained *via* the transformation $\chi_i = \sum_j \phi_{ij}X_j$, where φ_{ij} is the diagonalizing matrix of M_{ij} such that $\sum_{jk} \phi_{ij}M_{jk}\phi_{kl}^{-1} = \frac{\gamma_i}{\gamma}\delta_{il}$. γ_i's are the relaxation rates of the individual Rouse modes and they are normalized by the relaxation rate due to the harmonic interactions $\gamma = \mu\zeta$. The coarse-grained Fokker–Planck equation for the probability density $\rho(X_{\text{COM}},t)$ in terms of the polymer's center of mass, $X_{\text{COM}} = \chi_0/\sqrt{N}$, is then obtained by integrating out the orientation vectors $\{p_i(t)\}$ and the other Rouse modes $\{\chi_i(t); i \neq 0\}$ under a small gradient approximation as

$$\frac{\partial\rho}{\partial t} = -\nabla \cdot (\rho\mathscr{V} - \nabla(\mathscr{D}\rho)), \tag{3}$$

where the gradients are with respect to the center of mass coordinates. The complete Fokker–Planck equation and the coarse-graining procedure can be found in the ESI.† The effective drift $\mathscr{V}$ and diffusive coefficient $\mathscr{D}$ are functions of X_{COM} and are given by

$$\mathscr{V}(X_{\text{COM}}) = \frac{\tau}{dN}\left(\frac{S_1 + S_2}{2}\right)\nabla(v^2(X_{\text{COM}}))$$

$$\mathscr{D}(X_{\text{COM}}) = \frac{1}{N}\left(D + \frac{\tau}{d}S_2 v^2(X_{\text{COM}})\right) \tag{4}$$

with $\tau = 1/[(d-1)D_r]$, and $v(x)$ being the swim speed of ABP's ($v = \mu f_s$). S_1 and S_2 are given by

$$S_1 = \sum_{l=1, j=0}^{N-1} \frac{1}{1+\tau\gamma_l}\phi_{lj}^2\alpha_j^2, \quad S_2 = \frac{1}{N}\sum_{j=0}^{N-1}\alpha_j. \tag{5}$$

S_2 is the fraction of monomers that are active in the polymers while S_1 is a summation that involve the eigenvector matrix ϕ_{ij} and the re-scaled eigenvalues $\{\gamma_i\}$. We note that the dynamic

equation for the center of mass of the active polymer is determined by the dimensionless scaling or activity parameter

$$\kappa = \tau\gamma = \frac{\tau}{\tau_m}, \tag{6}$$

which denotes the ratio of persistence time of the direction of the activity with respect to the diffusive monomer relaxation time, $\tau_m = 1/\gamma$.

One can see in eqn (4) that the diffusivity of the polymer is enhanced due to activity compared to its all-passive counterpart (in which case the effective diffusivity would have been D/N) and the enhancement is proportional to the fraction S_2 of active monomers in the polymer. The effective drift $\mathscr{V}$ is generated by the gradient of the swim force squared, and is otherwise absent in passive or even constant activity systems. The steady state density of the center of mass of the polymer chain can now be calculated using the zero flux condition in (3) and the fact that $\mathscr{V} = \left(1 - \frac{\varepsilon}{2}\right)\nabla\mathscr{D}$, where

$$\varepsilon = \frac{S_2 - S_1}{S_2}. \tag{7}$$

In particular, we obtain-

$$\rho(X_{\text{COM}}) \propto \left[1 + \frac{\tau S_2 v^2(X_{\text{COM}})}{dD}\right]^{-\varepsilon/2}. \tag{8}$$

This tells us that the localization of polymers in response to activity is governed by the exponent ε, which encapsulates the competition between the effective drift, which causes the directed motion toward high activity regions, and effective diffusion, which tends to displace the polymer from its residing place. In particular, it is the sign of ε (or $S_2 - S_1$) that determines whether a polymer prefers to localize in high or low activity regions. For $\varepsilon < 0$, the density profile grows with the activity profile leading to preferential accumulation in high activity regions which is known as chemotaxis, while for $\varepsilon > 0$, the polymers accumulate in regions of low activity, leading to anti-chemotaxis.

Fig. 2 shows the steady state density profiles of various configurations of polymers for chain lengths $N = 6$ and $N = 18$, in an environment with a sinusoidal fuel concentration. Let us first consider the density distribution of polymers with a single active monomer compared to that with all monomers active. A polymer with only an end active monomer shows stronger accumulation in high activity regions compared to a polymer composed uniquely by active units. However, if the active monomer is located in the interior of the chain, the polymer's localization is weaker than an all-active polymer. This can be explained by the value of the exponent ε, which as mentioned before determines the location and effectiveness of the preferential accumulation. Precisely, the more negative is the value of ε, the more efficient is the accumulation of polymer in high activity regions. Therefore, by evaluating the values of ε (eqn (7)), we see that $|\varepsilon_{\text{end}}| > |\varepsilon_{\text{all}}| > |\varepsilon_{\text{interior}}|$ which supports the results presented in Fig. 2, which holds good independent
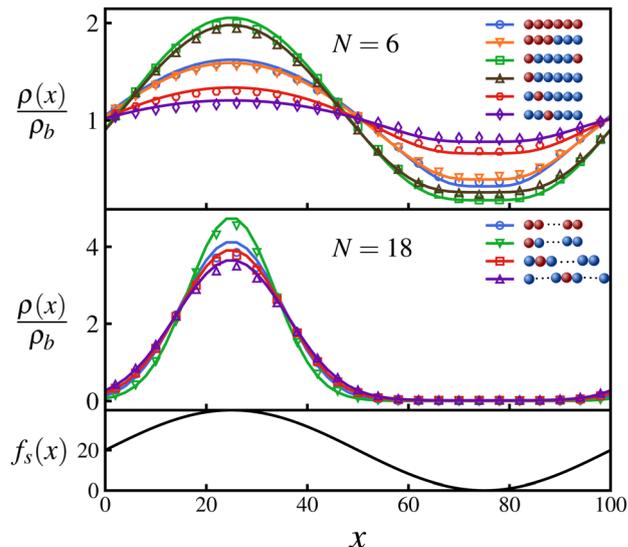

Fig. 2 The steady state density profiles for various configurations of a polymer with chain length $N = 6$ and $N = 18$ for $\zeta = 8$, $D_r = 5$, $\mu = 1$, and $D = 1$ in a box of length $L = 100$ that has a sinusoidally varying activity profile in the x-direction: $f_s(x) = 20\left(1 + \sin\left(\frac{2\pi x}{L}\right)\right)$ as depicted. The densities are normalized by $\rho_b = 1/L$. The solid lines represent analytical predictions and the symbols represent Langevin dynamics simulation results.

of the polymer length, as can be seen from the results for $N = 18$ in Fig. 2.

The limit $N \gg 1$ can be considered analytically for selected configurations of chains with one active monomer. In this case the summations in eqn (5) can be transformed into integrals leading to closed analytic expressions as shown in the ESI.† In particular we obtain for ε:

$$|\varepsilon_{\text{end}}| = \frac{N}{4\sqrt{\kappa}} - 1 \simeq 2|\varepsilon_{\text{mid}}|, \tag{9}$$

where "mid" denotes the center monomer. Similarly, we can solve the case of the all-active chain with the result: $\varepsilon_{\text{all}} \simeq \varepsilon_{\text{mid}}$. For chemotactic behavior ($\varepsilon < 0$) we require $N^2 \gg \kappa$, or $\tau \ll \tau_m N^2 = \tau_R$, which means that the active persistence time should be much smaller than the diffusive relaxation time, or Rouse time τ_R, of the whole chain. This result is in agreement with previous findings for all-active chains.[41]

Using the symmetry of the eigenfunctions of the connectivity matrix for the linear chain (see ESI†) we draw some further general conclusions about the role of the position of the active monomers inside the chain: Consider polymers that have a symmetric distribution of active monomers along the chain, e.g., a polymer with both terminal monomers active, and their corresponding antisymmetric polymers in which the active monomers are present in only one of half of the chain, e.g., for the above mentioned case is a polymer chain with only one end monomer active. Using the fact that the absolute values of the elements of the eigenvectors form a palindromic set, we can show that the values of S_1 and S_2 (eqn (5)) for a symmetric polymer are twice of those of its corresponding antisymmetric polymer. This leads to the same epsilon value (eqn (7)) for both
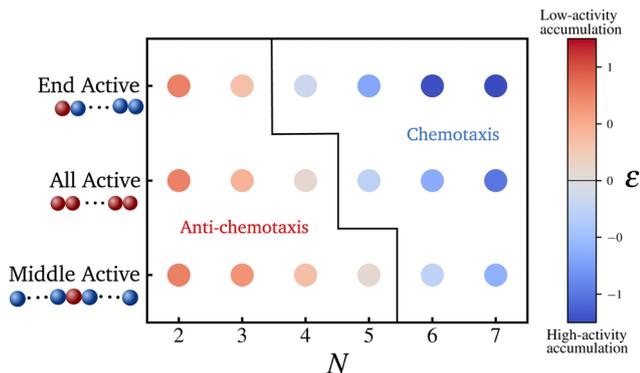
Fig. 3 Scatter plot for ε which indicates the location and degree of preferential accumulation for three distinct configuration of polymers of various chain length. Values of ε obtained analytically for the set of parameters mentioned in Fig. 2. As mentioned in the main text, $\varepsilon < 0$ on the colorbar indicates accumulation in high activity regions, and those greater than zero represent low-activity accumulation.

Fig. 4 The mean first passage time taken by a polymer to travel to the most active location starting from $x = L/2$ vs. the chain length of the polymer for four different configurations (other parameters are same as those specified in Fig. 2). The solid lines are theoretical predictions while the symbols are from Langevin dynamics simulations.

cases and as a result, their steady state densities differ only marginally due to the difference in the pre-factor in eqn (8), as can be seen in Fig. 2. This further emphasizes the fact that accumulative behaviour is largely determined by ε and shows that such a pair of symmetric–antisymmetric polymers have similar localization with respect to inhomogeneous activity.

Therefore, limiting our focus to polymers with just one or all monomers active, we construct in Fig. 3 a state diagram of the accumulation behavior of hybrid polymers. In particular, we consider polymers with different chain lengths N and three different configuration: active end monomer active, active central monomer active, and all monomers active. We observe that the switch from accumulation in lower activity regions to higher activity regions, for a given set of parameter values (ζ, μ, τ), can be achieved not only by increasing the chain length or varying the connectivity matrix as reported in ref. 41 but also by altering the number and positions of the active monomers within the polymer. Note that when all the monomers are active ($\alpha_i = 1$ for all i), the expression for the steady state density simplifies to the one presented in ref. 41 for polymers made up of Active Ornstein Uhlenbeck particles (AOUP's).[71,72] This illustrates that the accumulative behavior of polymers is not dependent on the specific model of active particles considered. Our findings remain robust for semiflexible polymers with small bending stiffness. For a detailed study on the effect of bending interactions, one can refer the ESI.†

Though eqn (8) gives us the steady state accumulation of various polymer chains, it does not give any insights into their dynamic behaviour, for example how fast do they get to the regions of high fuel concentration. In this direction, we solve for the mean first passage time (MFPT) $T(x)$, x being the initial position of the polymer's center of mass, the equation for which is obtained using the coarse-grained Fokker–Planck equation as[68]

$$\left(\left(1 - \frac{\varepsilon}{2}\right)\partial_x \mathscr{D}\right)\partial_x T(x) + \mathscr{D}\partial_x^2 T(x) = -1. \quad (10)$$

Setting $t_m = T(50)$ for a box of length $L = 100$, we calculate the average time taken by a polymer to reach the location of highest
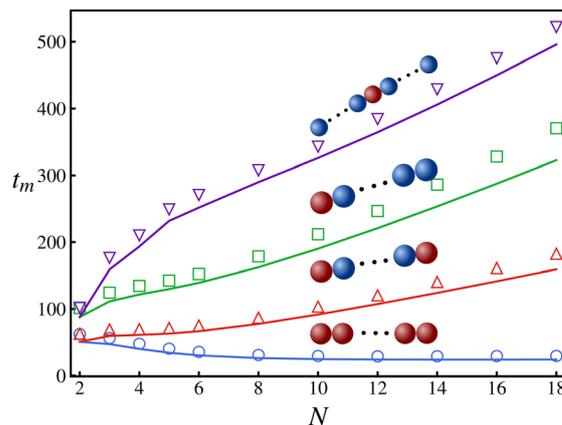
activity by imposing absorbing boundary conditions.[68] The results for the mean first passage time for various polymer configurations are presented in Fig. 4. For a polymer with all monomers active, the MFPT decreases as we increase the number of monomers, becoming nearly independent of the chain length for $N > 10$. However, other polymers with one or two monomers active take longer to reach the region of highest activity. As can be evinced from Fig. 4, the MFPT of polymers with a single active monomer varies depending on the position of the latter along the chain, reaching the minimum value when the active monomer is an end monomer. Furthermore, in contrast to the previously discussed accumulation behavior, Fig. 4 shows that introducing a further active monomer in a symmetric position compared to a preexisting one (as shown by the green and red solid lines in Fig. 4) has a tangible impact on the MFPT. In particular, the configuration with two monomers (red lines) is much faster compared to the other (green line). These results suggest that increasing the number of active units within a polymer decreases its MFPT.

Constructing a qualitative state diagram that encapsulates both the agility (defined as the inverse of MFPT) and the preferential accumulation behavior of polymers in Fig. 5, we get a comprehensive picture regarding hybrid polymers in chemical gradients. There seems to be no correlation between preferential accumulation and the mean first passage time of the polymers. We can therefore have polymers ranging from those that accumulate in high activity regions but are slow getting there (like long polymers ($N > 10$) with a sole interior monomer active) to those that are fast in getting to the high active regions but do not prefer to localize there (like relatively short polymers ($N = 4$) with all monomers active).

From our studies, we can therefore suggest strategies for polymerization that leads to (i) maximum accumulation and (ii) fastest motion, for a given N. A polymer with both terminal monomers active would result in the former while the one with all units active would be the fastest. This information may shed
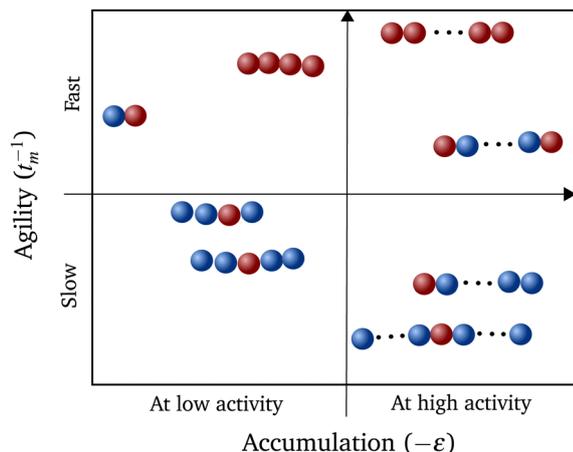
Fig. 5 A qualitative state diagram that illustrates the two studied properties of various polymers: (i) location of accumulation on the x-axis – by taking the negative of ε and (ii) mean first passage time of polymers to reach the location of highest activity t_{m}.

light onto the evolutionary development of important biopolymers like actin[73,74] and tubulin,[75] even though the form of activity at these length scales are different. The best strategy required for the function of the biopolymer can still be constructed by altering the number and position of the active units within the polymer. Similar self-localization of symmetric and corresponding anti-symmetric polymers can also be an indicator of introduction of asymmetry in biopolymers during evolution to yield an energy efficient directed transport.

The resulting directed transport in our work is an emergent property. While one could explicitly couple particle orientation to the local activity gradient, dependent on the specific activity mechanism, this would introduce an additional effect beyond the one in our study. We have also focused on polymers of fixed lengths. The incorporation of polymerization and depolymerization into a dynamical model is left for a future work. Our findings can also be coupled with existing studies on polymerization induced phase separation to study the formation and behaviour of active cell organelles[76] in future works.

Data availability

The code and primary data can be found at **https://zenodo.org/records/14825768** with **https://doi.org/10.5281/zenodo.14825768**.

Conflicts of interest

There are no conflicts to declare.

Acknowledgements

Notes and references

1 F. Müller, *Ecol. Modell.*, 1998, **108**, 3–21.
2 T. M. Keenan and A. Folch, *Lab Chip*, 2008, **8**, 34–57.
3 M. Almonacid, W. W. Ahmed, M. Bussonnier, P. Mailly, T. Betz, R. Voituriez, N. S. Gov and M.-H. Verlhac, *Nat. Cell Biol.*, 2015, **17**, 470–479.
4 M. Guthold, X. Zhu, C. Rivetti, G. Yang, N. H. Thomson, S. Kasas, H. G. Hansma, B. Smith, P. K. Hansma and C. Bustamante, *Biophys. J.*, 1999, **77**, 2284–2294.
5 B. Alberts, A. Johnson, J. Lewis, M. Raff, K. Roberts and P. Walter, *Bray D. Cell movements: from molecules to motility*, Garland Science, 2nd edn, 2000.
6 A. Javer, Z. Long, E. Nugent, M. Grisi, K. Siriwatwetchakul, K. D. Dorfman, P. Cicuta and M. Cosentino Lagomarsino, *Nat. Commun.*, 2013, **4**, 3003.
7 S. C. Weber, A. J. Spakowitz and J. A. Theriot, *Proc. Natl. Acad. Sci. U. S. A.*, 2012, **109**, 7338–7343.
8 A. Zidovska, D. A. Weitz and T. J. Mitchison, *Proc. Natl. Acad. Sci. U. S. A.*, 2013, **110**, 15555–15560.
9 M. Di Pierro, D. A. Potoyan, P. G. Wolynes and J. N. Onuchic, *Proc. Natl. Acad. Sci. U. S. A.*, 2018, **115**, 7753–7758.
10 S. F. Banani, H. O. Lee, A. A. Hyman and M. K. Rosen, *Nat. Rev. Mol. Cell Biol.*, 2017, **18**, 285–298.
11 J.-U. Sommer, H. Merlitz and H. Schiessel, *Macromolecules*, 2022, **55**, 4841–4851.
12 S. Ramaswamy, *Annu. Rev. Condens. Matter Phys.*, 2010, **1**, 323–345.
13 S. Ramaswamy, *J. Stat. Mech.: Theory Exp.*, 2017, **2017**, 054002.
14 G. De Magistris and D. Marenduzzo, *Phys. A*, 2015, **418**, 65–77.
15 É. Fodor, C. Nardini, M. E. Cates, J. Tailleur, P. Visco and F. Van Wijland, *Phys. Rev. Lett.*, 2016, **117**, 038103.
16 G. Gompper, R. G. Winkler, T. Speck, A. Solon, C. Nardini, F. Peruani, H. Löwen, R. Golestanian, U. B. Kaupp and L. Alvarez, *et al.*, *J. Phys.: Condens. Matter*, 2020, **32**, 193001.
17 F. Jülicher, S. W. Grill and G. Salbreux, *Rep. Prog. Phys.*, 2018, **81**, 076601.
18 M. C. Marchetti, J.-F. Joanny, S. Ramaswamy, T. B. Liverpool, J. Prost, M. Rao and R. A. Simha, *Rev. Mod. Phys.*, 2013, **85**, 1143–1189.
19 C. P. Brangwynne, G. H. Koenderink, F. C. MacKintosh and D. A. Weitz, *J. Cell Biol.*, 2008, **183**, 583–587.
20 W. Lu, M. Winding, M. Lakonishok, J. Wildonger and V. I. Gelfand, *Proc. Natl. Acad. Sci. U. S. A.*, 2016, **113**, E4995–E5004.
21 A. Ravichandran, G. A. Vliegenthart, G. Saggiorato, T. Auth and G. Gompper, *Biophys. J.*, 2017, **113**, 1121–1132.
22 C. A. Weber, R. Suzuki, V. Schaller, I. S. Aranson, A. R. Bausch and E. Frey, *Proc. Natl. Acad. Sci. U. S. A.*, 2015, **112**, 10703–10707.
23 R. G. Winkler, J. Elgeti and G. Gompper, *J. Phys. Soc. Jpn.*, 2017, **86**, 101014.

24 R. G. Winkler and G. Gompper, *J. Chem. Phys.*, 2020, **153**, 040901.

25 S. K. Anand and S. P. Singh, *Phys. Rev. E*, 2018, **98**, 042501.

26 R. E. Isele-Holder, J. Elgeti and G. Gompper, *Soft Matter*, 2015, **11**, 7181–7190.

27 C. A. Philipps, G. Gompper and R. G. Winkler, *J. Chem. Phys.*, 2022, **157**, 194904.

28 E. Locatelli, V. Bianco and P. Malgaretti, *Phys. Rev. Lett.*, 2021, **126**, 097801.

29 A. Kaiser and H. Löwen, *J. Chem. Phys.*, 2014, **141**, 044903.

30 C. Zhang, C. Xie, W. Feng, H. Luo, Y. Liu and G. Jing, *New J. Phys.*, 2023, **25**, 043029.

31 C. J. Anderson, G. Briand, O. Dauchot and A. Fernández-Nieves, *Phys. Rev. E*, 2022, **106**, 064606.

32 J. Harder, C. Valeriani and A. Cacciuto, *Phys. Rev. E*, 2014, **90**, 062312.

33 S. M. Mousavi, G. Gompper and R. G. Winkler, *J. Chem. Phys.*, 2021, **155**, 044902.

34 J. Shin, A. G. Cherstvy, W. K. Kim and R. Metzler, *New J. Phys.*, 2015, **17**, 113008.

35 M. Foglino, E. Locatelli, C. Brackley, D. Michieletto, C. Likos and D. Marenduzzo, *Soft Matter*, 2019, **15**, 5995–6005.

36 V. Bianco, E. Locatelli and P. Malgaretti, *Phys. Rev. Lett.*, 2018, **121**, 217802.

37 L. Natali, L. Caprini and F. Cecconi, *Soft Matter*, 2020, **16**, 2594–2604.

38 J.-X. Li, S. Wu, L.-L. Hao, Q.-L. Lei and Y.-Q. Ma, *Phys. Rev. Res.*, 2023, **5**, 043064.

39 M.-B. Luo and Y.-F. Shen, *Soft Matter*, 2024, **20**, 5113–5121.

40 H. D. Vuijk, H. Merlitz, M. Lang, A. Sharma and J.-U. Sommer, *Phys. Rev. Lett.*, 2021, **126**, 208102.

41 P. L. Muzzeddu, A. Gambassi, J.-U. Sommer and A. Sharma, *Phys. Rev. Lett.*, 2024, **133**, 118102.

42 L. Caprini, U. M. B. Marconi, R. Wittmann and H. Löwen, *Soft Matter*, 2022, **18**, 1412–1422.

43 A. Wysocki, A. K. Dasanna and H. Rieger, *New J. Phys.*, 2022, **24**, 093013.

44 J. R. Howse, R. A. Jones, A. J. Ryan, T. Gough, R. Vafabakhsh and R. Golestanian, *Phys. Rev. Lett.*, 2007, **99**, 048102.

45 H. Löwen, *Europhys. Lett.*, 2018, **121**, 58001.

46 J. Elgeti, R. G. Winkler and G. Gompper, *Rep. Prog. Phys.*, 2015, **78**, 056601.

47 C. Bechinger, R. Di Leonardo, H. Löwen, C. Reichhardt, G. Volpe and G. Volpe, *Rev. Mod. Phys.*, 2016, **88**, 045006.

48 R. Dreyfus, J. Baudry, M. L. Roper, M. Fermigier, H. A. Stone and J. Bibette, *Nature*, 2005, **437**, 862–865.

49 A. Najafi and R. Golestanian, *Phys. Rev. E: Stat., Nonlinear, Soft Matter Phys.*, 2004, **69**, 062901.

50 H.-R. Jiang, N. Yoshinaga and M. Sano, *Phys. Rev. Lett.*, 2010, **105**, 268302.

51 I. Theurkauff, C. Cottin-Bizonne, J. Palacci, C. Ybert and L. Bocquet, *Phys. Rev. Lett.*, 2012, **108**, 268303.

52 L. F. Valadares, Y.-G. Tao, N. S. Zacharia, V. Kitaev, F. Galembeck, R. Kapral and G. A. Ozin, *Small*, 2010, **6**, 565–572.

53 M. J. Schnitzer, *Phys. Rev. E*, 1993, **48**, 2553.

54 A. Sharma and J. M. Brader, *Phys. Rev. E*, 2017, **96**, 032604.

55 H. C. Berg, *E. coli in Motion*, Springer, 2004.

56 M. Schnitzer, S. Block and H. Berg, *Biology of the chemotactic response*, 1990, vol. 46, pp. 15.

57 H. C. Berg, *Random walks in biology*, Princeton University Press, 1993.

58 I. R. Lapidus, *J. Theor. Biol.*, 1980, **86**, 91–103.

59 F. Peng, Y. Tu, J. C. Van Hest and D. A. Wilson, *Angew. Chem., Int. Ed.*, 2015, **54**, 11662–11665.

60 P. K. Ghosh, Y. Li, F. Marchesoni and F. Nori, *Phys. Rev. E*, 2015, **92**, 012114.

61 H. D. Vuijk, A. Sharma, D. Mondal, J.-U. Sommer and H. Merlitz, *Phys. Rev. E*, 2018, **97**, 042612.

62 H. Merlitz, H. D. Vuijk, R. Wittmann, A. Sharma and J.-U. Sommer, *PLoS One*, 2020, **15**, e0230873.

63 H. D. Vuijk, S. Klempahn, H. Merlitz, J.-U. Sommer and A. Sharma, *Phys. Rev. E*, 2022, **106**, 014617.

64 P. L. Muzzeddu, H. D. Vuijk, H. Löwen, J.-U. Sommer and A. Sharma, *J. Chem. Phys.*, 2022, **157**, 134902.

65 P. L. Muzzeddu, É. Roldán, A. Gambassi and A. Sharma, *EPL*, 2023, **142**, 67001.

66 B. Valecha, P. L. Muzzeddu, J.-U. Sommer and A. Sharma, *arXiv*, 2024, preprint, arXiv:2409.18703, DOI: **10.48550/arXiv.2409.18703**.

67 J.-U. Sommer and A. Blumen, *J. Phys. A: Math. Gen.*, 1995, **28**, 6669.

68 C. W. Gardiner, *Springer series in synergetics*, 1985.

69 H. Risken, *The Fokker–Planck Equation*, 1996.

70 M. Doi, S. F. Edwards and S. F. Edwards, *The theory of polymer dynamics*, oxford university press, 1988, vol. 73.

71 D. Martin, J. O'Byrne, M. E. Cates, É. Fodor, C. Nardini, J. Tailleur and F. Van Wijland, *Phys. Rev. E*, 2021, **103**, 032607.

72 L. Caprini and U. M. B. Marconi, *Soft Matter*, 2018, **14**, 9044–9054.

73 F. Straub, *Stud. Inst. Med. Chem., Univ. Szeged*, 1943, **3**, 23–37.

74 S. Y. Khaitlina, *Biochemistry*, 2014, **79**, 917–927.

75 E. Hamel and C. M. Lin, *Biochemistry*, 1984, **23**, 4173–4184.

76 C. A. Weber, D. Zwicker, F. Jülicher and C. F. Lee, *Rep. Prog. Phys.*, 2019, **82**, 064601.